Surface induced reactivity for titanium by ion implantation

M. T. PHAM, H. REUTHER, W. MATZ, R. MUELLER
Forschungszentrum Rossendorf e.V., Institut für Ionenstrahlphysik und Materialforschung, Postfach 510119, D-01314 Dresden, Germany
E-mail: pham@fz-rossendorf.de

G. STEINER
Technische Universität Dresden, Institut für Analytische Chemie, D-01062 Dresden, Germany

S. OSWALD
Institut für Festkörper–und Werkstofforschung, Postfach 270016, D-01171 Dresden, Germany

I. ZYGANOV
Staatliche Technische Universität Lipezk, Lehrstuhl für Physikalische Metallkunde, ul. Moskowskaja, 398055 Lipezk, Russia

Calcium and phosphorus storage in a thin layer of titanium surface was achieved by ion implantation. We study the reactivity of this surface in response to a hydrothermal treatment. The incipient implanted species are observed to convert to Ca^{2+} and PO_4^{3-}, the precursors for generating calcium phosphate polymorphs. Hydroxyapatite is formed from these precursors by an interface-liquid mediated mineralization preceded by the hydrolysis of oxygen compounds of Ca and P from the solid phase. The morphology and organization of apatite mineral is controlled by the fluid dynamics reflecting the surface remodeling to adapt to the available local environment. Exposed to calcium and phosphate ion containing solution, the hydrothermally treated surface templates hydroxyapatite deposition. Ca and P implanted Ti surface was shown to be chemically and morphologically actively involved in the interfacial reactions.

1. Introduction

Artificial biomaterials used in orthopaedic and dental surgery traditionally employ stainless steels and Ti alloys. They are either bioinactive or their degree of bioactivity is insufficient. Inadequate osseointegration [1] and a high level metal ion release [2] have been known as a result of this lack of biocompatibility. Surface coating with bioactive ceramics [3] presents a potential alternative to tailor combined beneficial properties: ceramic biocompatibility with mechanical toughness of metals. Bioactive ceramics bond to bone via an intermediate apatite-containing layer [4]. Synthetic analog to crystalline bone mineral hydroxyapatite (HA) is the important ceramic used for coatings to mimic this fact. HA coatings have been shown to improve bone bonding [5] and the barrier effect on metal ion release from the base metal substrate [6].

HA coatings can be achieved by a variety of techniques [7–17]. One limitation is the difficulty of engineering the interfacial bond strength coating-substrate. The inherent nature of the methodology, common to all coating techniques, results in distinct interfaces critically susceptible to load triggered fractures and with attachment strength dictated by the adhesion of HA to the substrate. This has been overcome to some extent with the interface mixing by ion beams [12]. Another critical limitation is the difficulty in achieving a surface coating truely mimicking all aspects of a biologically produced interface material.

A strategy attempted in the present report is to endow the Ti surface with precursors capable of being actively involved in the tissue bonding reactions. This route is *in vitro* tested in this paper studying the behavior of Ca and P stored in the Ti surface. Surface-stored Ca and P are achieved by ion-implantation in controllable concentration, distribution, and penetration. The reactivity of such ion–implanted surfaces is examined in response to a hydrothermal oxidation which provides the oxidation of Ca and P, and simulates the formation of calcium phosphates in an aqueous interfacial environment. Our results show that the primaryly implanted species are converted to CaO, P_2O_5, Ca^{2+} and PO_4^{3-}, the precursors for generating various calcium phosphate polymorphs. Furthermore, hydroxyapatite is formed from these precursors by an interface-liquid mediated mineralization preceded by the hydrolysis of oxygen compounds of Ca and P from the solid phase. This process, equivalent to the deposition from solution, involves surface

remodeling to adapt to the available local environment reflecting the controlling fluid dynamics. In Ca^{2+} and PO_4^{3-} ions containing medium, the partially HA-doped surface templates HA growing from solution.

2. Materials and methods

Samples studied are plates of pure Ti, $12 \times 12 \times 1\,mm^3$ (Goodfellow). One face was polished to a metallographic finish using an aqueous silica suspension. Ca and P were sequentially implanted into the Ti surface. The total ion doses used are 1.8×10^{17} and 9×10^{16} ions/cm^2 for Ca and P, respectively. To reach an approximately homogeneous distribution, the implantation was conducted in several energy steps at 55, 42, 30 and 25 keV for Ca and 40, 30 and 20 keV for P. The hydrothermal treatment was carried out in a water vapor autoclave at 120, 150, 170, and 200 °C.

Samples were studied by X-ray diffraction (XRD), scanning electron microscopy (SEM) X-ray photoelectron spectroscopy (XPS), auger electron spectroscopy (AES), Fourier transform infrared spectroscopy (FTIR) and FT-Raman scattering. The elemental composition and surface chemistry was studied with AES and XPS. The XPS/AES system used is a Microlab 310F system. The depth profiles were taken at intervals of argon sputtering (3 keV Ar ions, current density of 2 μA/cm^2). The total sputtered depth was measured for each sample by a profilometer (Dektak 800, VEECO, USA). Assuming an averaged sputter rate, the depth scale was obtained for depth profiling. Core level XPS spectra were measured for O 1s, Ti 2p, Ca 2p, P 2p and C 1s. Energy calibration was achieved by setting the hydrocarbon C 1 s line at 284.6 eV. FTIR spectroscopy was carried out on a Brucker IFS 88 Specard with reflection unit. The angle of incidence was 80°. FT-Raman spectra were collected using a DILOR XY spectrometer. All the results were referenced to the unimplanted Ti surface. XRD measurements were performed on a step scan diffractometer in grazing incidence geometry $\omega = 1°$ using a thin film attachment and CuK_α radiation. The counting time per step and the step size were 15–30 s and 0.1°, respectively. Samples as prepared were used directly in XRD measurements without any further treatment. The morphology study was performed by scanning electron microscopy using a DSM 962 (Carl Zeiss/Oberkochen, Germany). The element distribution was measured with EDX (Noran/Voyager 1000).

3. Results and discussion

3.1. Element depth distribution

The surface constituting elements distributed along depth perpendicular to the surface plane are obvious from sputter depth profiles (Fig. 1). The contaminant C found only in the outermost surface, less than 5 nm, is omitted in the diagrams. Ca and P in the as-implanted sample (Fig. 1a), are seen to be incorporated within the Ti matrix with their homogeneous distribution over the major surface depth consistent with the multi-energy implantation regime used in the preparation. The integration of the profiles gives a Ca-to-P ratio of ca. 2.1 reasonably corresponding to the nominal implantation dose ratio of

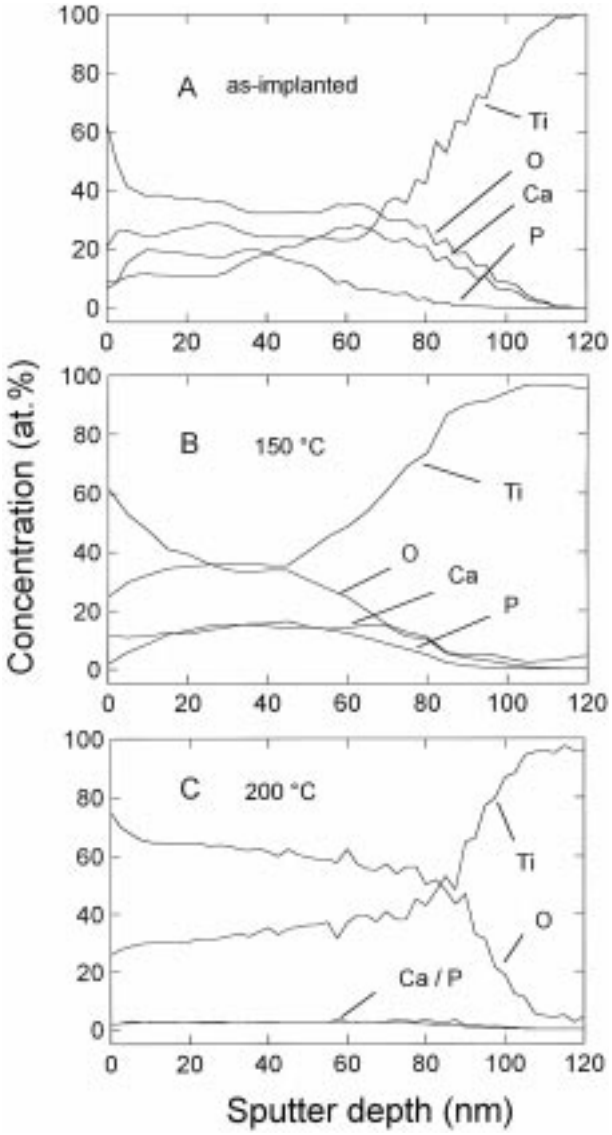

Figure 1 Element depth profiles of the Ti surface after implantation with $1.8 \times 10^{17} Ca^+/cm^2$ and $9 \times 10^{16} P^+/cm^2$ (A) and hydrothermal oxidation at 150 °C (B) and 200 °C (C) for 2 h.

2.0. Oxygen is observed to follow the Ca penetration, presumably due to oxidation of Ca during implantation [18, 19]. The amount of oxygen accounts for only about 28% of the expected value corresponding to a complete oxidation to form stoichiometric CaO, P_2O_5, and TiO_2. We deduce that P, the most inreactive, with respect to oxygen binding affinity, among the components under study (Ca, P, Ti), is partially oxidized after ion implantation. In general, crystallite features protruding from the surface after extensive hydrothermal treatment (see below) endows the surface heterogenous. The depth profiles of samples obtained after oxidation, (Fig. 1b and c), are shown therefore for selected regions with no crystallite features. Following oxidation the surface is depleted from Ca and P to an extent depending on temperature. After a 200 °C hydrothermal treatment the surface appears to be largely titanium oxides with P and Ca present only in trace amounts. At this stage, large needle-like crystallites of Ca phosphate (see below) were observed on the surface suggesting that Ca and P stored in the implanted layer have been extracted in favor of

interface reactions to form calcium phosphates. The mobility of Ca and P may be the result of their oxygen compounds reacting with water and forming ionic species. The matrix seems stable since the layer thickness for which Ca and P were found, is comparable before and after treatment. The overall result reveals a surface picture delineated by an outermost feature of calcium phosphate mediated by a TiO_x transition region toward the base Ti metal.

3.2. Surface chemistry

3.2.1. Oxygen related components

Fig. 2 shows the O 1 s spectra (from top to bottom: 200 °C-, 170 °C-, 150 °C-oxidized, as-implanted, and virgin surface). The O 1 s region of the virgin surface reveals the surface TiO_2 by the major peak at 530.2 eV [20, 21]. An asymmetrical, well visible broadening toward the higher binding energy side reflects two other oxygen containing species resulting from the hydroxylation of the TiO_2 surface [21–23]. These are the acidic bridged hydroxyl groups associated with oxygens doubly coordinated with titanium (531.6 eV) and the basic terminal hydroxyl groups associated with oxygens singly coordinated (533.3 eV).

Oxygen involved in various bonding states corresponding to different chemical surface species is additionally observed from the O 1 s spectra as a result of implantation and oxidation. For the as-implanted surface the most significant alterations imprinted by ion implantation are on the high energy spectrum side and are convincingly recognized by the growing signal intensity with increasing implantation dose. The shoulder at ca. 529.9 eV is the residue of the TiO_2 peak well-nigh submerged by virtue of the occurence of other prevalent surface components. The binding energies may have contributions with overlapping values, since no spectrum features displaying discernible peaks are seen. Surface species contributing to the convoluted binding energy spectrum observed involve 531.7 eV CaO [24, 25], 531.4 eV $CaCO_3$ [26], 131.2 eV $CaTiO_3$ [24]. The vertical bars in the figure indicate the listed energy positions. Although the present analysis provided no quantitively unambiguous identification, oxides and hydroxide of Ca and Ti may be the most dominant oxygen containing surface species produced in the as-implanted state. First, the oxygen depth profiles and the characteristics of core level spectra of Ti 2p, Ca 2p, and P 2p (see below), together with other results, reasonably fit to this picture. Second, oxide and hydroxide of Ca have been identified to be the major products generated by Ca implantation into Ti [24, 19].

For implanted samples exposed to hydrothermal oxydation the major alterations are observed on the high binding energy side suggesting two groups of surface components resulting from the oxidation. The first group relates to the products (see above) of the TiO_2 hydroxylation that, although common for the virgin surface used, but extensively proceeds under the water vapor exposure at elevated temperature und pressure. The O 1 s spectra obtained for control samples without implantation (virgin surface) clearly confirms this fact, demonstrating that the hydroxylation products modify the spectrum features only quantitatively. Similar characteristics have been known from hydration experiments on Ti using aqueous solutions [20]. Referring to this starting point, it becomes apparent that the massive changes observed in the spectra are attributed to the second group of surface species as a result of reactions of implanted Ca and P. Among them, further oxidation of Ca and P, hydrolysis of their oxidation products, formation of Ca phosphates and HA, phase transformation, and amorphous-crystalline conversion are the possible reactions. The convoluted O 1 s spectum features reflect their various products exhibiting closely spaced binding energies. The surface components, in addition to the TiO_2 hydroxylation products, that may contribute to the observed behavior refer, if ordered in increasing ernergy, to $CaTiO_3$ (531.2 eV) [24], $CaCO_3$ (531.4 eV), $CaHPO_4 \cdot 2H_2O$ (531.5 eV), HA (531.7 eV) [19], CaO (531.7 eV), $Ca(HPO_4)_2 \cdot H_2O$ (533.0 eV) [25]. Hydroxyapatite is one major product of these, in agreement with the results of XRD, FTIR, FT-Raman (see below). With increasing temperature, the high binding energy components are observed to grow in intensity. At 200 °C, the highest applied temperature, peak features appear even higher than that of TiO_2. The temperature controlled process is obvious from the development of energy peak intensity of HA and calcium phosphates relative to TiO_2 suggesting that their amount becomes larger with temperature consistent with microscopic observations and XRD results. Evaluating the energy peak areas reveals that ca. 25% of TiO_2 are left in the outermost surface pointing to two aspects. The first is

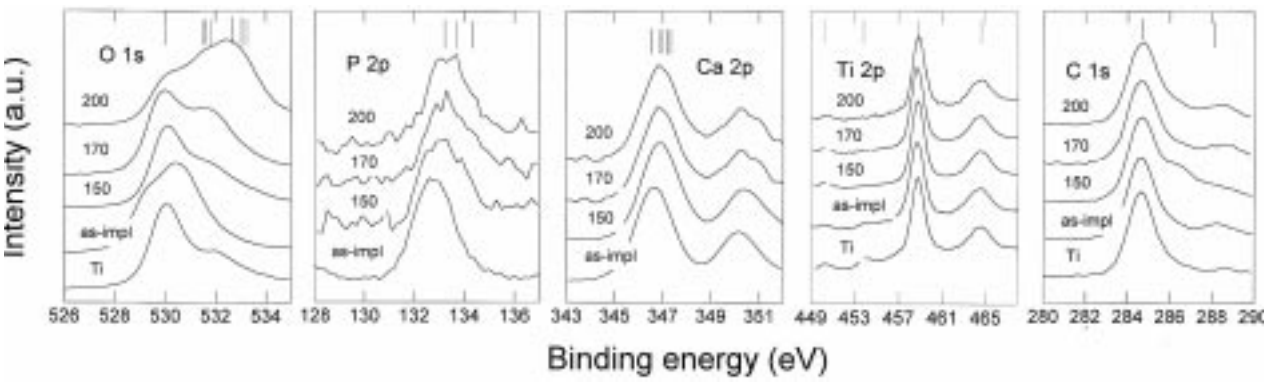

Figure 2 XPS core level spectra (from left to right) of O 1 s, P 2p, Ca 2p, Ti 2p and C 1 s for Ti surface in virgin state, after Ca + P implantation, and after implantation + hydrothermal oxidation. The vertical bars indicate the energy positions characteristic of surface species detailed in the text.

that the new phase introduced by ion implantation, including HA, is embedded in the TiO_2 matrix in contrast to closed film overlayers obtained by other techniques. The second implies that as-implanted species are only partially oxidized with respect presumably to P that needs four O each to form PO_4 groups.

3.2.2. Phosphorus related components

The P 2p regions in Fig. 2 show from top to bottom: 200 °C-, 170 °C-, 150 °C-oxidized, and as-implanted surfaces. P is seen to be involved prevalently in its mono- and pentavalent-oxidation states corresponding to hypophosphite (P^+) and phosphate (P^{5+}) signalized by singlets at 132.2 eV and 133.3 eV binding energy [27]. Note that elemental (red) phophorus (P^0) has a 2p doublet at 129.9 eV binding energy [26] and negative valence in phosphides displaying 2p energies below 128 eV [19, 28]. The spectra are increasingly asymmetrical toward the higher binding energy side on going from as-implanted to oxidized. Some tendency of shifting peak energy toward higher values is observed with oxidation and rising oxidation temperature, reaching a reduced broadening at the highest applied treatment temperature, 200 °C. This behavior suggests that (i) several P-containing species are formed with closely spaced binding energy values, (ii) continuation of the oxygen uptake, and (iii) conversion among these components resulting in enrichment of a stable component upon thermal treatment. The transition from as-implanted to oxidized appears to imprint no distinctive alterations (producing no new peak features) on the core level spectra suggesting that the nearest chemical environment around P formed due to implantation remains unchanged after oxidation treatment. With the reaction mixture under study (P, Ca, O and Ti) phosphates and hydrogen phosphates are the most probable products to be expected. The P containing surface species having 2p energies reasonably matching to the P 2p spectra obtained include HA (133.2–133.5 eV) [25, 29], $CaHPO_4 \cdot 2H_2O$ (133.7 eV) [25], $Ca(H_2PO_4) \cdot H_2O$ (134.3 eV) [25]. The listed energy positions are indicated by vertical bars in the figure. The convergent tendency toward 133.4 eV observed in the spectra and the prevalent Ti-O bonding (see above) justify the conclusion that HA represents a major surface component among others.

3.2.3. Calcium related components

The core level spectra for Ca 2p are shown in Fig. 2, from top to bottom: 200 °C-, 170 °C-, 150 °C-oxidized and as-implanted surface. The as-implanted surface has the typical doublet peak feature at 346.6 eV ($2p_{3/2}$) and 350.2 eV ($2p_{3/2}$) with a spin orbit splitting of 3.6 eV [30]. This behavior provides evidence for divalent Ca containing surface species ($2p_{3/2}$ energy for elemental Ca is at 345.7 eV [30]). The symmetrical and featureless spectra generally known for the insensitivity of the core level spectrum Ca 2p toward variation in chemical environment [31] do not permit species identification. Ca containing surface species whose Ca $2p_{3/2}$ energies fall into the energy region of the observed spectra may be $CaTiO_3$ (346.5 eV) [24], CaO (346.8–347.2 eV) [24, 26, 30], HA (347.2–347.6 eV) [19, 32], $CaHPO_4 \cdot 2H_2O$ (347.4 eV) [25], $CaCO_3$ (347.0 eV) [26, 33]. After hydrothermal oxidation no discernible alterations are seen regarding spectrum feature and FWHM (full width at half maximum). The $2p_{3/2}$ energy position appears to shift, although weakly, toward the higher energy side after oxidation. The degree tends to increase with increasing oxidation temperature. The Ca $2p_{3/2}$ peak values are 346.8 eV, 347.0 eV and 347.5 eV for 150 °C, 170 °C and 200 °C, respectively. The tendency observed fits reasonably to the picture supporting Ca involved increasingly in HA and Ca phosphates due to the conversion via hydrothermal process.

3.2.4. Titanium related components

Core level spectra of Ti 2p were recorded for the virgin surface and the implanted surface before and after hydrothermal oxidation. The results are presented in Fig. 2, from top to bottom: 200 °C-, 170 °C-, 150 °C-oxidized, as-implanted and virgin surface. TiO_2 is seen to be the only Ti containing species present on all surfaces as evidenced by the Ti 2p regions indicating two main peaks at 458.7 eV ($2p_{3/2}$) and 464.6 eV ($2p_{1/2}$), characteristic of TiO_2 with a spin orbit splitting of 5.9 eV [34]. The parent metal Ti buried underneath the oxide overlayer is visible by the peak at 453.8 eV ($2p_{3/2}$), only weakly for the virgin surface, turning indistinctively after implantation, and disappearing after oxidation. The tendency is obvious that implantation and oxidation lead to oxide overlayers growing beyond the native oxide thickness, ca. 4 nm [20], consistent with the oxygen depth profiles. The peak feature around 450 eV arises from $K_{3,4}$ satellites of the X-ray used. The fact that the binding energies of Ti 2p, all displaying values identical to those of the starting Ti surface, suggests that oxygen is the prevalent nearest chemical environment of Ti also for the implanted surface and after hydrothermal oxidation. Moreover, Ca and P do not undergo reactions with Ti, the outermost surface revealing no reaction products from them. The great reactivity of Ti toward O (high negative free energy of TiO_2 formation–203.8 kcal/mol) explains its preferential oxidation. $CaTiO_3$ is another likely compound beside the major TiO_2 to be expected from the reaction system under study composing of Ti, Ca, P and O. Its Ti $2p_{3/2}$ binding energy of 458.4 eV [24] coincides with that of TiO_2, thus XPS-unidentifiable. Its amount, if present, may be negligible in view of Ca prevalently involved in reactions with O and P (see below).

3.2.5. Carbon related components

The C 1 s core level spectra are presented in Fig. 2, from top to bottom: 200 °C-, 170 °C-, 150 °C-oxidized, as-implanted and virgin surface. The virgin surface reveals trace carbon as evidenced by the energy peak at 284.6 eV typical of adventitious carbon originating from hydrocarbon contamination due to XPS analysis [35]. Following implantation a new resolved subpeak additionally appears at 288 eV implying that this further C

containing component comes from carbonate [36]. The carbonate carbon has its origin from atmospheric CO_2 due to reactions with CaO, $Ca(OH)_2$ and $CaTiO_3$ known as vigorous CO_2 scavengers. Evidence for surface carbonate is confirmed furthermore in a sample only–Ca implanted displaying a distinct energy peak at 288 eV. Quantitatively the C containing species are negligible (ca. 15% relative to the trace carbon) and collect exclusively in the outermost surface as apparent from the depth profiles. Once formed, surface carbonate seems to stop efficiently the CO_2 penetration. The implanted surface after hydrothermal oxidation displays no new features in the C 1 s region. Some tendency toward alleviating peak intensity and resolvability of the spectrum around the carbonate energy region suggests the occurence of other competing reactions and some degree of conversion of $CaCO_3$ in other species, e.g. carbonated apatite. A slight asymmetry in spectrum, toward the higher energy side, is generally observed in all cases that is rather due to vibrational fine structure [37] than signalizing any new surface species.

3.2.6. FTIR and FT-Raman analysis

Supportive and complementary results regarding the surface chemistry were obtained from FTIR and FT-Raman spectroscopic measurements. The as-implanted sample, (Fig. 3a, upper trace), displays absorption bands at 1100, 1050 and 963 cm^{-1} consistent with the asymmetric (ν_3) stretching modes and the symmetric P-O stretching mode of HA [38–42]. The band at 560 cm^{-1} corresponds to the antisymmetric bending motion of phosphate groups in HA [38–42]. The bands at $\sim$ 3600 cm^{-1} and 632 cm^{-1} are consistent with the stretching mode and the vibration mode, respectively, of OH^- ions in HA [39–42]. The typical spectral features of HA become more obvious after hydrothermal oxidation (Fig. 3a, lower trace) suggesting the conversion towards HA. The spectrum characteristics suggest further P containing species: pyrophosphate $P_2O_7^{2-}$ at 753 cm^{-1} [43], β–tricalcium phosphate at 975 and 948 cm^{-1} [40] and HPO_4^{2-} at 875 cm^{-1} [42, 44]. Surface carbonate, a trace contamination, is observed by CO_3^{2-} bands in the region of 1600 to 1300 cm^{-1} due to ν_3 vibrational mode carbonate ions and by the band at 873 cm^{-1} due to the ν_2 vibrational mode [45]. The bands at 3660 cm^{-1} and 875 cm^{-1} may indicate the presence of $Ca(OH)_2$ and CaO.

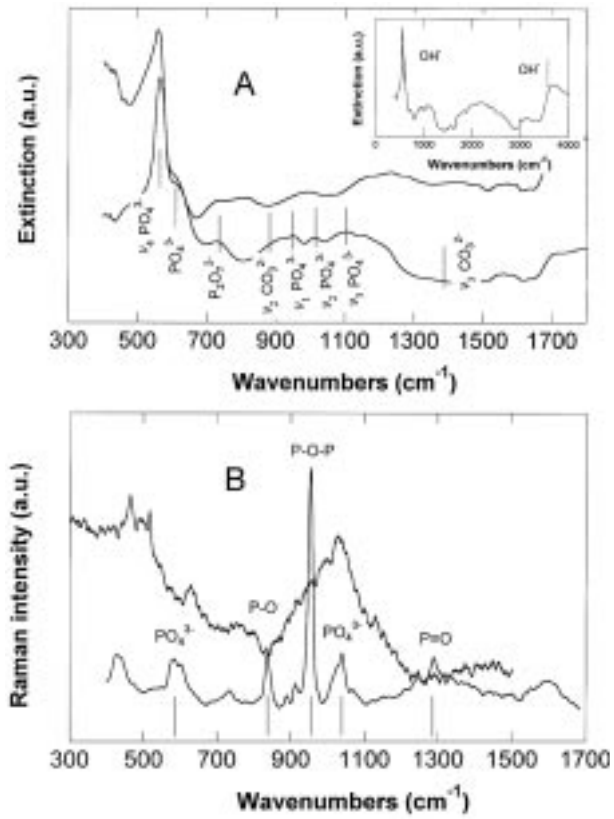

Figure 3 FTIR (A) and FT-Raman (B) spectra of a Ca and P implanted Ti surface after hydrothermal treatment at 200 °C for 2 h. Upper traces are respective records for the as-implanted surface. The inset shows absorption bands of OH^- at 3570 and 633 cm^{-1} from HA. Vertical bars indicate the wavenumber positions characteristic of HA, phosphates, and carbonate.

The FT-Raman spectra are presented in Fig. 3b. The as-implanted sample (upper trace) exhibits a broad band around 1200–900 cm^{-1} suggesting a convolution of some closely spaced energy bands. HA is known to produce characteristic bands at 1144, 959 and 773 cm^{-1} [46]. The FT-Raman spectrum of the sample exposed to hydrothermal treatment (Fig. 3b, lower trace) reveals surface HA being prevalent. From this comparison, HA is deduced to be one component of the surface. The intense band at 1000 cm^{-1} and a series of weaker bands near 700, 600 and 460 cm^{-1} suggest that Ti–substituted apatite and Ti phosphate ($Ti(HPO_4)_2nH_2O$) [46] are further surface species. The FT-Raman spectrum of the sample exposed to hydrothermal treatment (Fig. 3b) reveals surface HA being prevalent.

3.3. Phase analysis

Results of the XRD analysis are shown in Fig. 4. For the as-implanted sample (Fig. 4a) Ti is observed to dominate the spectrum feature corresponding to the polycrystalline Ti phase of the starting substrate. Three other crystalline phases identifiable from the diffraction patterns appear in minor quantities. The first component relates to the two-valent titanium oxide, TiO (PDF-No. 12-754 [47]). It seems reasonable due to competing Ca and P present in excess leading to an oxygen deficient surface. The oxygen deficiency, referenced to the total O amount corresponding to stoichiometric TiO_2, CaO and P_2O_5, was evident from the element depth profiles, (see above) Only titanium and TiO are clearly evidenced by the diffraction patterns. There remains some very small peaks in the spectrum. Candidates for explaining them are $Ca_2Ti_5O_{12}$ (PDF-No. 33-315 [47]) and Ti_5P_3 phase (PDF-No. 45-888 [1]). Because of the small amount of these crystals in the implanted region the identification is ambiguous. From these results we deduce that (i) oxygen compounds of Ca with P (exposed and buried), as followed from the XPS analysis, are amorphous or finely crystalline to escape an X-ray scattering, (ii) all the XRD observed phases are buried underneath the surface, since other surface species were identified by XPS that is surface specific due to its small sampling depth of below ca. 5 nm, whereas XRD has a penetration depth of about 250 nm.

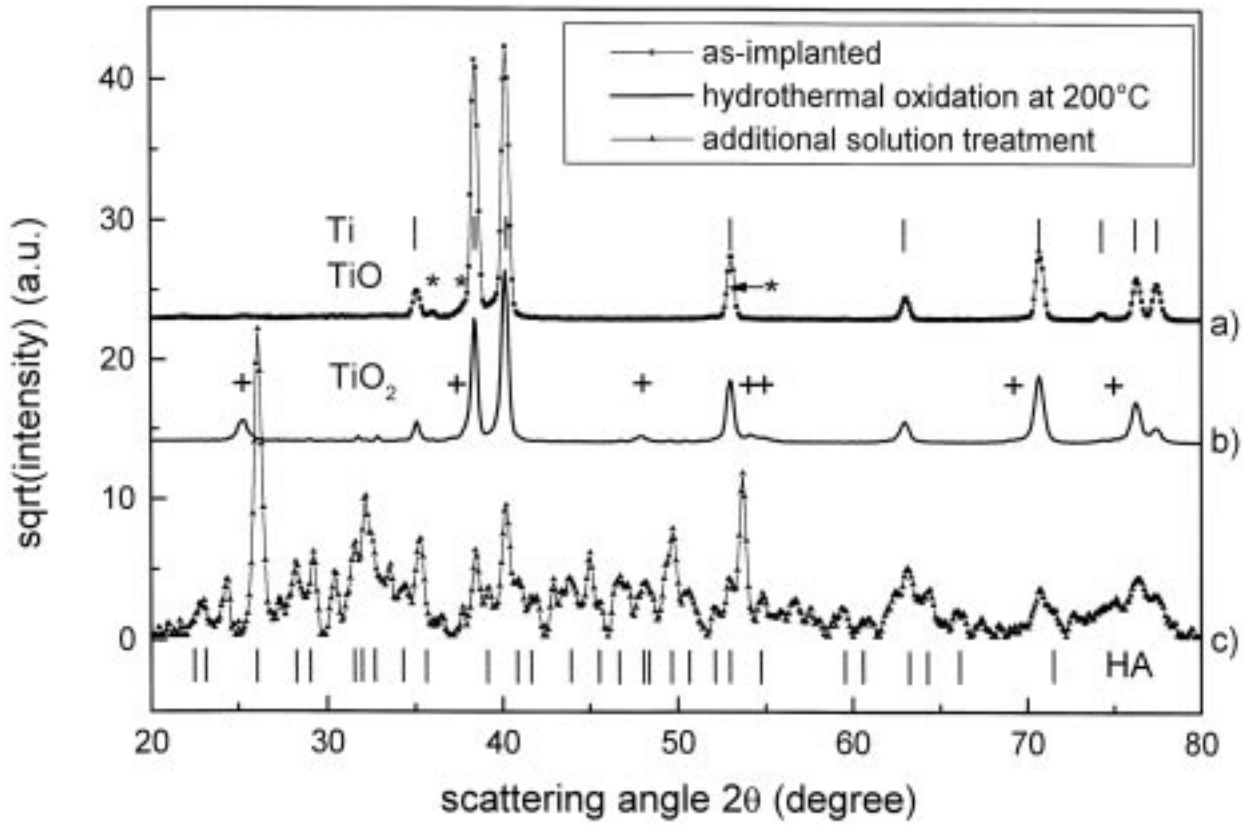

Figure 4 XRD patterns of titanium implanted with Ca and P and subsequently heat treated. (a) as-implanted state; (b) hydrothermal oxidation at 200 °C for 2 h; (c) additional treatment in a Ca^{2+} and PO_4^{3-} containing solution at 37 °C for 5 h. The ordinate is in the square-root of intensity scale to display the small peaks better. In spectrum (c) some unidentified peaks remain.

Samples exposed to a hydrothermal oxidation at different temperatures reveal diffraction patterns like that shown in Fig. 4b for a sample after a 200 °C treatment. Only two crystalline phases are visible on the spectrum now; they are the substrate Ti and TiO_2 anatase (PDF-No.21-1272 [47]). The relative intensity of these two phases suggests that a considerable amount of the surface Ti has been oxidized by the treatment with the low-valent Ti contribution becoming negligible. There is no evidence for any Ca and P containing crystalline phases. We recall that at this stage needle-like crystallites appear on the surface (see morphology) and a depletion of Ca and P from the implanted layer in favor of the formation of Ca-P compounds on the outermost surface (see element distribution + surface chemistry). We speculate that the crystalline needles present on the surface (ca. $8 \times 10\,mm^2$ sample area) are in a concentration insufficient for XRD detection used here. Moreover they appear in a form like whiskers and may be well oriented. In such a case powder diffraction arrangement is only by accident able to detect Bragg reflections from such a substance.

To additionally enhance the needle-like crystalline phase, after oxidation treatment the sample was exposed to a calcium-ion and phosphate-ion containing solution at 37 °C for 5 h (2.5 mM Ca^{2+} and 1 mM HPO_4^{2-} at pH 7.4). The XRD analysis provided diffraction patterns, (Fig. 4c), consistent with a hydroxyapatite phase (PDF-No. 9-432 [47]). An unimplanted control sample experiencing the same procedure revealed only amorphous material. We conclude that the needle-like crystallites primarily formed due to oxidation are of hydroxyapatite origin that template the additional deposition from solution. The morphology examination (see morphology) confirmed that the crystal phase after solution growing displays simimlar appearence to that after oxidation. But the number of crystals seems greater and they have more statistical orientation distribution. This now allows detection by XRD.

3.4. Surface morphology

The needle-like structure is the prevalent feature of the morphology observed on all implanted surfaces followed by a hydrothermal treatment. Control samples without ion implantation did not show such a structure implying that it relates to the reaction products of implanted Ca and P. Such a morphology is characteristic of hydroxyapatite precipitated from chloride-free solution containing Ca^{2+} and HPO_4^{2-} ions [48–50]. Results from SEM studies are presented in Fig. 5. The back-scattered electron image (Fig. 6) reveals a distinct contrast with the Ti substrate indicating the local enrichment of Ca and P in the crystal features observed in the secondary electron topographical image. This provides further evidence for the reaction of Ca with P. The X-ray maps demonstrate that the components involved in the needle crystals are Ca, P and O. Evidence for the formation of oxygen compounds is seen furthermore by the line scan of the oxygen EDX signal obtained across a crystal needle. The formation of the crystalline phase is observed to occur readily at

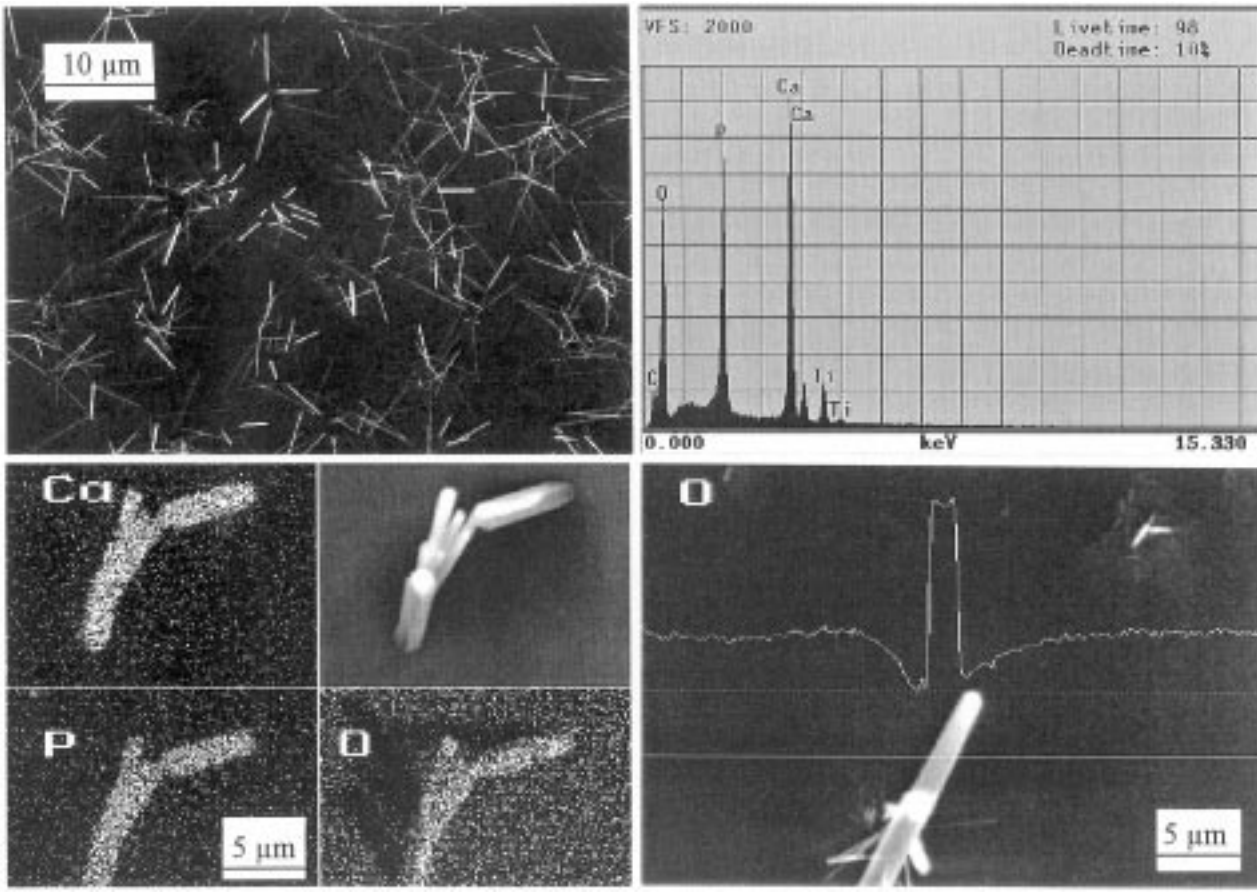

Figure 5 HA needle crystals formed by hydrothermal treatment from Ca and P implanted in Ti. SEM image and EDX spectrum (upper), EDX maps for Ca, P and O distribution and oxygen EDX signal across a crystal needle (lower).

120 °C, the lowest value in our experiment series. A temperature increase, up to 200 °C, produced no new crystal feature, but revealed a growth in size and concentration. Under the present experimental conditions HA has proved to be the most stable form preferentially being formed among the calcium phosphates. The amorphous to crystalline transformation for HA is kinetically inhibited and the temperature effect is to accelerate this process. An induction period of 3.5 min has been reported for crystalline HA appearing from the amorphous phase at 70 °C in solution precipitation experiments [48]. We emphasize the oxidative aspect in the present work to completely convert implanted Ca and P to their oxidation state corresponding to CaO and P_2O_5. The surface density and size of the crystals are seen to be controlled by the nominal implanted dose of Ca for a fixed Ca to P ratio of 2: the more the greater the ion dose. The crystal needles are randomly oriented, but aligned their long axes along the substrate surface plane. Some surface regions are populated with few separated large crystals.

Crystals randomly assembled to disordered multi-

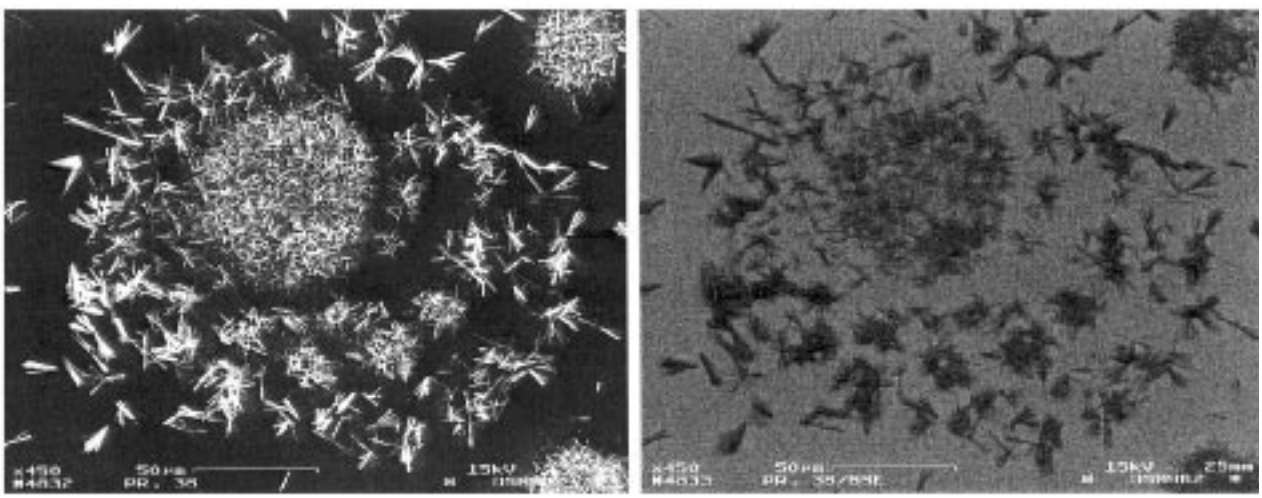

Figure 6 Secondary (left) and back scattered (right) electron images of a Ca and P implanted surface after hydrothermal treatment at 200 °C for 2 h.

layered aggregates are also observed that in turn are arranged to ornamentally concentric spheres (Fig. 6). This picture reveals that the nucleation and growth occur at the interface with the aqueous phase mediating the formation and transport of the necessary precursor ions. The implanted layer presents the supplier for the latter. The liquid dynamics (condensation and removal of water droplets during the course of the hydrothermal treatment) generating a variety of local environments for the crystal nucleation, growth and assembly will thus explain the ornaments observed.

3.5. Model reactions of the interface mineralization

The Ti surface implanted with Ca and P was shown to be chemically composite. Oxygen compounds of Ca, P and Ti present the main fractions composed of CaO, P_2O_5 and TiO_2. The outermost surface is contaminated with $Ca(OH)_2, CaCO_3, PO_4^{3-}$ and Ti-OH due to reactions with atmospheric CO_2 and H_2O. Other components buried beneath the surface relate to low valent P (P_2O_3, Ti_5P_3) and Ti (Ti_2O_3, TiO).

The reactivity of this surface was demonstrated using hydrothermal treatment, revealing its ability to generate apatite calcium phosphates. Three stages of the process events may be suggested to understand the reactions involved. The first stage involves the oxidation of P^{3-}, P^0 and P^{3+} to complete the P_2O_5 formation. The low valence of the P fraction is deduced from the XPS results and indirectly from the oxygen deficiency found in the element depth profiles of as-implanted samples. Ca is assumed to be readily in its maximum oxidation state as CaO corresponding to the Ca 2p core level spectra. The penetration depth of Ca at the low implantation energies used (< 50 keV) appears to be still within the range of the surface oxidation during the implantation (elemental calcium was observed, e.g. for 200 keV implantation due to the penetration depth exceeding the surface oxidation range). The subsequent stages are mediated by the liquid phase with the reactions occuring at the interface water (water vapor) and implanted surface. The second stage is associated with the formation of the ion precursors Ca^{2+}, PO_4^{3-} and H^+ by the hydrolysis of oxides yielding a supersatured solution phase immediately sticking on the surface. The final stage involves the nucleation and growth of calcium phosphate from this interface solution film to form HA. This process regulates the supersaturation and presents the driving force for supplying new ion precursors from beneath the surface. Initially the spontaneous hydrolysis and the lack of a seeding crystalline phase may produce a high supersaturation level associated with amorphous calcium phosphate. The crystalline HA inexceptionally observed in the present experiments is consistent with its fast amorphous to crystalline transformation [51]. A transformation induction time of some minutes has been reported [48].

The ion implanted Ti surface was shown to be capable of converting to a HA containing composite structure under optimized conditions that are equivalent to those of the precipitation from solution. The interface mediated HA formation observed reveals, moreover, a strategy for surface mineralization from precursors stored in the solid and *in situ* released upon exposure to the biological environment. An extended material thickness, adjustable by the implantation parameters, is involved in the surface remodeling process. This would result in an interface bonding more favorable than that of the pure film coatings. Some indications are seen from the present work. All crystal features remained unchanged after exposure to an intensive sonical bath in water (or alcohol, acetone) for 30 min. The ion precursors readily available from the solid phase may facilitate the mineralization of the interface. Many ornaments of the crystal features observed in these experiments reflect the adaptation of the growing phase to the local environments. Water droplets and vapor covering surface regions are such local spaces produced during the hydrothermal process.

4. Conclusions

Titanium surfaces capable of being actively involved in biomineralization can be produced by storing Ca and P within a thin layer of its surface, as repository of precursors for generating calcium phosphates. This is achieved using ion implantation. The reactivity of such a surface is manifested by the conversion of the incipient implanted species into CaO, P_2O_5, Ca^{2+}, PO_4^{3-} and hydroxyapatite. The stages of conversion cover oxydation, hydrolysis, precipitation, and crystallization, which can be controlled to produce stage precursors and the target HA. Hydrothermal treatment is an example demonstrating the conversion resulting in a HA doped Ti surface. HA is formed in an interface process mediated by liquid-solid phase reactions. The morphology and organization of this apatitic interface mineralization are shown to be controlled by the interfacial fluid dynamics reflecting the adaptation to available local environments. An arrested conversion into intermediate stage precursors is feasible and an improved tissue bonding is conceivable by inducing an *in situ* formation of HA from precursors released from the solid phase. *In vivo* test experiments remain to be conducted.

Acknowledgments

We thank Mrs G. Küster for her assistance with the optical microscopic experiments. We are grateful to Dr Schoeneich and his team for their ion implantation work.

References

1. L. SENNERBY, L. E. ERICSON, P. THOMSEN, U. LEKHOLM and P. ASTRAND, *Clin. Oral. Implant Res.* **2** (1991) 103.
2. K. E. HEALY and P. DUCHEYNE, *J. Mater. Sci.: Mater. Med.* **4** (1993) 117.
3. E. MUNTING, M. VERHELPEN, F. LI and A. VINCENT, in ''CRC handbook of bioactive ceramics'', edited by T. Yamamuro, L. L. Hench and J. Wilson (CRC Press, Boca Raton, MA, 1990) p. 143.
4. K. OHURA, T. YAMAMURO, T. NAKAMURA, T. KPKUBO, Y. EBISAWA, Y. KOTUORA and M. OKA, *J. Biomed. Mater. Res.* **25** (1991) 357.
5. M. GOTTLANDER and T. ALBREKTSSON, *Int. J. Oral Maxillofac. Jmp.* **6** (1991) 339.
6. P. DUCHEYNE, J. CUCKLER, S. RADIN and E. NAZAR, in ''CRC handbook of bioactive ceramics'', edited by T. Yamamuro,

L. L. Hench and J. Wilson (CRC Press, Boca Raton, MA, 1990) p. 123; S. R. SOUSA and M. A. BARBOSA, *J. Mater. Sci.: Mater. Med.* **6** (1995) 818.
7. S. R. RADIN and P. DUCHEYNE, *J. Mater. Sci.: Mater. Med.* **3** (1992) 33.
8. H. OGUCHI, K. ISHIKAWA, S. OJIMA, Y. HIRAYAMA, K. SETO and G. EGUCHI, *Biomaterials* **13** (1992) 471.
9. C. M. COTELL, D. B. CHRISEY, K. S. GRABOWSKI, J. A. SPRAGUE and C. R. GOSSETT, *J. Appl. Biomater.* **3** (1992) 87.
10. M. SHIRKHANZADEH, *J. Mater. Sci.: Mater. Med.* **6** (1995) 90.
11. P. DUCHEYNE, S. RADIN, M. HEUGHEBAERT and J. C. HEUGHEBAERT, *Biomaterials* **11** (1990) 244.
12. F. Z. CUI, Z. S. LUO and Q. L. FENG, *J. Mater. Sci.: Mater. Med.* **8** (1997) 403; Y. OHTSUKA, M. MATSUURA, N. CHIDA, M. YOSHINARI, T. SUMII and T. DERAND, *Surf. Coat. Technol.* **65** (1994) 224.
13. J. L. ONG, L. C. LUCCAS, W. R. LACEFIELD and E. D. RIGNEY, *Biomaterials* **13** (1992) 249.
14. X. DING, K. YAMASHITA and T. UMEGAKI, *J. Ceram. Soc. Jpn.* **103** (1995) 867.
15. J. B. STEVENSON, H. SOLNIK–LEGG and K. O. LEGG, *Mater. Res. Soc. Symp. Proc.* **110** (1989) 715.
16. J. A. JANSEN, J. G. C. WOLKE, J. P. C. M. VAN DER WAERDEN and K. DE GROOT, *Clin. Oral Implant Res.* **4** (1993) 28.
17. M. YOSHINARI, K. OZEKI and T. SUMII, *Bull. Tokyo Dent. Coll.* **32** (1991) 147.
18. E. WIESER, I. ZYGANOV, W. MATZ, H. REUTHER, S. OSWALD, M. T. PHAM, E. RICHTER, *Surf. Coat and Technol.* **111** (1999) 103.
19. T. HANAWA, H. UKAI, K. MURAKAMI and K. ASAOKA, *Materials Transactions, JIM* **36** (1995) 438.
20. K. E. HEALEY and P. DUCHEYNE, *Biomaterials* **13** (1992) 553.
21. T. K. SHAM and M. S. LAZARUS, *Chem. Phys. Lett.* **68** (1979) 426.
22. M. BROWNE, P. J. GREGSON and R. H. WEST, *J. Mater. Sci.:Mater. Med.* **7** (1996) 323.
23. R. O. ANSELL, T. DICKINSON, A. F. POVEY and P. M. A. SHERWOOD, *J. Electoanal. Chem. Interfacial Electrochem.* **10** (1979) 69; M. ARFELLI, G. M. INGO, G. MATTOGNO and A. M. BECCARIA, *Surf. Interface Anal.* **16** (1990) 299.
24. T. HANAWA, H. UKAI and K. MURAKAMI, *J. Electron Specstrosc. Relat. Phenom.* **63** (1993) 347.
25. T. HANAWA and M. OTA, *Biomaterials* **12** (1991) 767.
26. C. D. WAGNER, W. M. RIGGS, L. E. DAVIS, T. F. MOULDER and G. E. MUILENBERG, in ''Handbook of X-ray photoelectron spectroscopy'', edited by J. Christian (Perkin-Elmer: Norwalk, CT, 1978); C. D. WAGNER, in ''Practical surface analysis'', edited by D. Briggs and M. P. Seah (John Wiley & Sons, 1990) p. 595.
27. R. B. DIEGLE, N. R. SORENSEN, C. R. CLAYTON, M. A. HELFAND and Y. C. YU, *J. Electrochem. Soc.* **135** (1988) 1085; S. J. SPLINTER, R. ROFAGHA, N. S. MCINTYRE and U. ERB, *Surf. Interf. Analysis* **24** (1996) 181.
28. M. PALAVIN, D. N. HENDRICKSON, J. M. HOLLANDER and W. L. JOLLY, *J. Phys. Chem.* **74** (1970) 116; C. D. WAGNER and J. A. TAYLOR, *J. Electron. Specrosc.* **20** (1980) 83.
29. M. YOSHINARI, Y. OHTSUKA and T. DERAND, *Biomaterials* **15** (1994) 529.
30. H. VAN DOVEREN and J. A. TH. VERHOEVEN, *J. Elec. Spectrosc. Rel. Phenom.* **21** (1980) 265.
31. T. HANAWA and M. OTA, *Appl. Surf. Sci.* **55** (1992) 269.
32. S. ZHANG and K. E. GONSALVES, *J. Mater. Sci.:Mater. Med.* **8** (1997) 25.
33. D. R. LIDE, (Ed) ''Handbook of chemistry and physics'' (CRC Press, Boca Raton, FL, 1994).
34. M. SCROCCO, *Chem. Phys. Lett.* **61** (1979) 453.
35. J. KASPERKIEWICZ, J. A. KOVACICH and D. LICHTMAN, *J. Electron. Spectrosc. Rel. Phenom.* **32** (1983) 123.
36. C. MIOT, E. HUSSON, C. PROUST, R. ERRE and J. P. COUTURES, *J. Mater. Res.* **12** (1997) 2388; M. P. SEAH and W. A. DENCH, *Surf. Int. Anal.* **1** (1979) 2.
37. D. BRIGGS, J. C. RIVIERE, in ''Practical surface analysis'', edited by D. Briggs and M. P. Seah (John Wiley & Sons, New York, 1990) Vol. 1, p. 131.
38. J. M. STUTMAN, J. D. TERMINE and A. S. POSNER, *Trans. N.Y. Acad. of Sci.* **29** (1966) 669.
39. D. G. A. NELSON and J. D. B. FEATHERSTONE, *Calcif. Tissue Intern.* **34** (1982) 69; B. O. FOWLER, E. C. MORENO and W. E. BROWN, *Arch. Oral Biol.* **11** (1966) 477.
40. P. DUCHEYNE, W. VAN RAEMDONCK, J. C. HEUGHEBAERT and M. HEUGHEBAERT, *Biomaterials* **7** (1986) 97.
41. M. SHIRKHANZADEH, *J. Mater. Sci.: Mater. Med.* **6** (1995) 90.
42. S. R. RADIN and P. DUCHEYNE, *J. Biomed. Mater. Res.* **27** (1993) 35.
43. H. MONMA and T. KANAZAWA, *Yogyo-Kyokai-Shi* (The Ceram. Soc. Japan) **84** (1976) 209.
44. A. OSAKA, Y. MIURA, K. TAKEUCHI, M. ASADA and K. TAKANASHI, *J. Mater. Sci.: Mater. Med.* **2** (1991) 51; H. CHAAIR, J. C. HEUGHEBAERT and M. HEUGHEBAERTT, *J. Mater. Chem.* **5** (1995) 895; J. S. A. BETT, L. G. CHRITNER and W. K. HALL, *J. Amer. Chem. Soc.* **89** (1967) 5535.
45. M. VIGNOLES, G. BONEL, D. W. HOLCOMB and R. A. YOUNG, *Calcif. Tissue Intern.* **43** (1988) 33; I. REHMAN and W. BONFIELD, *J. Mater. Sci.: Mater. Med.* **8** (1997) 1.
46. C. C. RIBEIRO, M. A. BARBOSA, A. A. S. C. MACHADO, A. TUDOR and M. C. DAVIES, *J. Mater. Sci.: Mater. Med.* **6** (1995) 829; A. R. TUDOR, C. D. MELA, M. C. DAVIES, D. AADERSON, G. HASTINGS, S. MORREY, J. D. SANTOS and M. A. BARBOSA, *Spectrochim. Acta* **49** (1993) 675.
47. ''The powder diffraction file, set 1–46'', International Center for Diffraction Data, Newtown Square, PA 19073–3273.
48. D. WALSH, J. L. KINGSTON, B. R. HEYWOOD and S. MANN, *J. Crystal Growth* **133** (1993) 1.
49. J. MORADIAN–OLDAK, S. WEINER, L. ADDADI, W. J. LANDIS and W. TRAUB, *Connect. Tissue Res.* **25** (1991) 219.
50. B. R. HEYWOOD, N. H. C. SPARKS, R. P. SHELLIS, S. WEINER and S. MAMM, *Connect. Tissue Res.* **25** (1990) 1.
51. G. H. NANCOLLAS, in ''Biomineralization, chemical and biochemical perspectives'', edited by S. Mann, J. Webb and R. J. P. Williams (VCH, Weinheim, 1989) p. 157.

Received 27 August 1998
and accepted 29 April 1999